# Solitons in the one-dimensional antiferromagnet $CsCoBr_3$

S. E. Nagler
*Chalk River Nuclear Laboratories, Atomic Energy of Canada Limited, Chalk River, Ontario K0J 1J0, Canada and Department of Physics, University of Toronto, Toronto, Ontario M5S 1A7, Canada*

W. J. L. Buyers
*Chalk River Nuclear Laboratories, Atomic Energy of Canada Limited, Chalk River, Ontario K0J 1J0, Canada*

R. L. Armstrong
*Chalk River Nuclear Laboratories, Atomic Energy of Canada Limited, Chalk River, Ontario K0J 1J0, Canada and Department of Physics, University of Toronto, Toronto, Ontario M5S 1A7, Canada*

B. Briat
*École Supérieure de Physique et de Chimie Industrielles, 10 rue Vauquelin, F-75005 Paris, France*
(Received 17 January 1983; revised manuscript received 2 June 1983)

The soliton response occurring at elevated temperatures in the one-dimensional Ising-type antiferromagnet $CsCoBr_3$ has been studied by neutron scattering. An inelastic peak is observed and identified as the Villain mode arising from the propagation of domain walls. Calculations have been made of the response from domain-wall—pair states and an extension of the first-order perturbation theory derived by Ishimura and Shiba. A reasonable account is obtained of the observed polarization and intensity of the scattering. The effect of collisions is seen to be increasingly important as the temperature is raised. The response near the zone center has been compared with the ideal—soliton-gas theory of Maki. The theoretical prediction, which has the form of a Lorentzian raised to the power $\frac{3}{2}$, gives a good qualitative description of the temperature dependence of the intensity and width of the scattering.

## I. INTRODUCTION

It is now well established that solitons play an important role in the dynamics of one-dimensional (1D) magnetic systems. For example, the Hamiltonian of a chain of classical planar spins in a magnetic field can be reduced to a sine Gordon Hamiltonian.[1] The resulting solitons lead to a central peak which has been observed in neutron scattering experiments in ferromagnetic[2] ($CsNiF_3$) and antiferromagnetic[3] [$(CH_3)_4NMnCl_3$ (TMMC)] planar spin chains. A quantum system of particular interest where solitons can be observed in the absence of a magnetic field is the $S=\frac{1}{2}$ Ising-type antiferromagnetic chain. At low temperatures the spin excitations consist predominantly of pairs of domain walls separated by a lattice constant; these can be regarded as solitons of unit length. In addition, as first predicted by Villain,[4] domain walls may be thermally excited and should lead to a low-frequency component of the longitudinal neutron scattering. The scattering extends to a frequency where a square-root singularity occurs and which obeys a sinusoidal dispersion law. The existence of the central component in the scattering was noted in neutron experiments on the 1D magnet $CsCoCl_3$,[5] and in $CsCoBr_3$ (Ref. 6) the well-defined inelastic peak that corresponds to the Villain mode was observed for the first time. Shiba and Adachi[7] have shown how propagating domain walls can be studied using ESR as confirmed by experiment on $CsCoCl_3$.[8] This work contains a complete account of the $CsCoBr_3$ experiments briefly reported above. In addition, new calculations of $S(Q,\omega)$ for the 1D Ising-type antiferromagnet are presented.

Ishimura and Shiba[9] (IS) have calculated the $T=0$ spin-wave response of the 1D Ising-type antiferromagnet by considering domain-wall—pair states, or solitons, of all lengths. As shown below the perturbation theory from the Ising limit can be extended to finite temperature to calculate both the longitudinal and transverse "soliton" response. The calculation is complementary to that of Villain, and has the advantage of providing a unified description of the spin-wave and soliton scattering. It illuminates the connection between the single—domain-wall description of Villain and the domain-wall—pair description of Ishimura and Shiba.

The perturbation theory described above is valid for wave vectors near the zone boundary. Recently Maki[10] has suggested that near the antiferromagnetic zone center ($|Q-\pi| \ll \pi$), the longitudinal response of the Ising-type antiferromagnetic chain can be described by considering an ideal gas of solitons. The experimental results on $CsCoBr_3$ provide evidence for such ideal-gas behavior.

The paper is organized in the following manner: Section II contains the theoretical derivation of the soliton response. Next, the experiment is described. In Sec. IV the results are compared with theory and discussed in detail.

## II. THEORY

The magnetic component of the inelastic neutron scattering from a 1D system of localized spins is determined by the dynamical spin-correlation function,

$$S^{\alpha\alpha}(Q,\omega)=\int_{-\infty}^{\infty}\frac{dt}{2\pi}e^{-i\omega t}\langle S^{\alpha}_{-Q}(0)S^{\alpha}_{Q}(t)\rangle\ , \tag{2.1}$$

where $\alpha=x,y,z$ and $S^{\alpha}_{Q}=N^{-1/2}\sum_r e^{iQr}S^{\alpha}_r$ is the Fourier transform at wave-vector transfer $Q$ along the chains of the spin distribution over the sites $r$. If the eigenstates of the system $|E_i\rangle$ and the matrix elements between them are known exactly, or in some approximation, one can write

$$S^{\alpha\alpha}(Q,\omega)=Z^{-1}(\beta)\sum_{E_1,E_2}e^{-\beta E_1}|\langle E_2|S^{\alpha}Q|E_1\rangle|^2 \times\delta(\omega-E_2+E_1)\ , \tag{2.2}$$

where $\beta=1/k_BT$ and $Z(\beta)=\sum_{E_1}e^{-\beta E_1}$.

Consider the exchange Hamiltonian of the $S=\frac{1}{2}$ Ising-type antiferromagnet

$$\hat{H}=2J\sum_i S^z_iS^z_{i+1}+2J\epsilon\sum_i(S^x_iS^x_{i+1}+S^y_iS^y_{i+1})\ , \tag{2.3}$$

where $\epsilon$ lies between 0 and 1.

At low temperatures the effective $S=\frac{1}{2}$ Hamiltonian of the $CsCoX_3$ salts should also include[11] a term $h\sum_i(-1)^iS^z_i$ that describes an effective field $h$ that arises from both the exchange mixing of $Co^{2+}$ single-ion levels and the interchain interactions. At elevated temperatures this term has been shown to be unimportant[11] and is therefore ignored in what follows.

The ground state of $\hat{H}^{zz}$ is doubly degenerate and consists of the two Néel states $|N_1\rangle$ and $|N_2\rangle$ related by a spin reversal at every site. Consider a state $|n\rangle$ where the two parts of the chain are aligned in the ground configurations $|N_1\rangle$ and $|N_2\rangle$ separated by a domain wall between spins $n$ and $n+1$ (Fig. 1). The Ising energy of this state relative to the Néel state is given by $J$. When the term $\hat{H}^{xy}$ is included, the state $|n\rangle$ is coupled to states $|n\pm2\rangle$. As shown by Villain,[4] to first order in $\epsilon$ the eigenstates are given by

$$|Q\rangle=N^{-1/2}\sum_n e^{iQn}|n\rangle\ , \tag{2.4}$$

with $E_Q=J+2\epsilon J\cos2Q$.

The state $|Q\rangle$ corresponds to a domain wall propagating along the chain with a characteristic momentum $Q$. The velocity of a wall is given by

$$V_Q=\frac{\partial}{\partial Q}E_Q=-4\epsilon J\sin2Q\ . \tag{2.5}$$

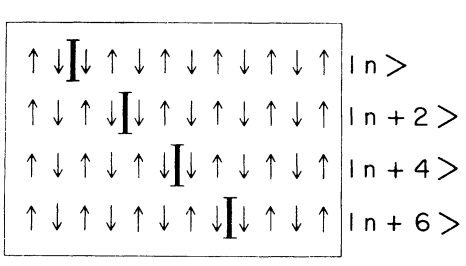


FIG. 1. Antiferromagnetic domain walls. The state $|n\rangle$ with a wall at position $n$ is coupled to the states $|n\pm2\rangle$.

A propagating domain wall in a strongly Ising-type chain can be called a soliton in the sense that it moves with a constant velocity and shape and connects two degenerate ground states.[12] It is not a sine Gordon soliton like those that give rise to a central component in 1D planar spin systems.[1-3] Villain[4] calculated the longitudinal correlation function $S^{zz}(Q,\omega)$ that gives the neutron scattering from states consisting of a single, thermally excited domain wall. Such single–domain-wall excited states can only occur in open-ended chains of spins.

For a chain with periodic boundary conditions, the lowest-lying excitations will occur close to the Ising energy $2J$. The relevant excited states can be obtained from a Néel state by flipping all spins in a block of $\nu$ adjacent sites so as to yield a domain-wall–pair state as shown in Fig. 2. When the number of spins $N$ is even, the Néel state has a total $z$ component of spin $S^z_T=0$ and the domain-wall–pair states can have $S^z_T=0,\pm1$. As shown below the scattering from thermally excited domain-wall–pair states has the same form as the single–domain-wall scattering calculated by Villain.[4] For this reason, and because the disturbance is the natural one under periodic boundary conditions, in this paper we shall refer to the domain-wall–pair states as solitons.

In analogy to the method of IS (Ref. 9) one can choose a set of basis states corresponding to domain-wall pairs propagating with wave vector $Q$. For periodic boundary conditions and an even number of spins $N\gg1$ one can write for states of $S^z_T=+1$ (odd $\nu$)

$$|\nu,Q\rangle_0=\left[\frac{2}{N}\right]^{1/2}\times\sum_j e^{iQj}\left[S^+_j\prod_{m=1}^{(\nu-1)/2}(S^-_{j+2m-1}S^+_{j+2m})\right]|N_1\rangle\ . \tag{2.6}$$

The $S^z_T=-1$ states are defined in an analogous fashion. There are two distinct types of $S^z_T=0$ (even $\nu$) states:

$$|\nu,Q\rangle_1=\left[\frac{2}{N}\right]^{1/2}\sum_j e^{iQj}\left[\prod_{m=0}^{\nu/2-1}S^-_{j+2m}S^+_{j+2m+1}\right]|N_1\rangle\ , \tag{2.7}$$

$$|\nu,Q\rangle_2=\left[\frac{2}{N}\right]^{1/2}\sum_j e^{iQj}\left[\prod_{m=0}^{\nu/2-1}S^+_{j+2m}S^-_{j+2m+1}\right]|N_1\rangle\ .$$

Within the restricted space consisting only of the domain-wall–pair (DWP) states, the matrix elements of $\hat{H}$ within each of the above types of states are given by

$$\langle\nu_2,Q_2|\hat{H}|\nu_1,Q_1\rangle=\delta_{Q_2,Q_1}(2J_{\nu_2,\nu_1}+V_{Q_1}\delta_{\nu_2,\nu_1-2}+V^*_{Q_1}\delta_{\nu_2,\nu_1+2}) \tag{2.8}$$

where $V_{Q_1}=\epsilon J(1+e^{-2iQ_1})$. Here $Q_1,Q_2$ correspond to the initial and final wave vectors and, since the matrix elements do not depend on the value of $S^z_T$, the external label on the state vectors has been dropped.

Diagonalizing Eq. (2.8) corresponds to first-order per-

$\uparrow\downarrow\uparrow\downarrow\uparrow\downarrow\uparrow\downarrow\uparrow\downarrow$ Néel State $S^z_T=0$

$\uparrow\downarrow\uparrow\downarrow\uparrow[\uparrow]\uparrow\downarrow\uparrow\downarrow$ $\nu=1$ $S^z_T=+1$

$\uparrow\downarrow\uparrow\downarrow[\downarrow\uparrow]\uparrow\downarrow\uparrow\downarrow$ $\nu=2$ $S^z_T=0$

$\uparrow\downarrow\uparrow\downarrow[\downarrow\uparrow\downarrow]\downarrow\uparrow\downarrow$ $\nu=3$ $S^z_T=-1$

FIG. 2. Examples of domain-wall–pair (DWP) states. Domains of length $\nu$ flipped from the Néel state of $S^z_T=0$ can have $S^z_T=\pm1$ for odd $\nu$ and $S^z_T=0$ for even $\nu$.

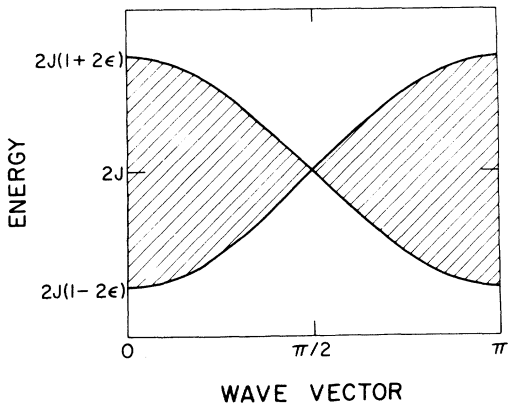


FIG. 3. Excitation continuum. The upper and lower bounds are given by $2J(1\pm2\epsilon\cos Q)$.

turbation theory on the Hamiltonian Eq. (2.3), treating $\hat{H}^{xy}$ as a perturbation. As pointed out by IS, for a given value of $Q_1$ the matrix elements of Eq. (2.8) are equivalent to those of a tight-binding model with free ends, where the nearest-neighbor transfer integral is $V_{Q_1}$. For the intraband problem considered here, the boundary condition is unimportant. However, the condition is important for the calculation of the $T=0$ spin-wave response, which involves interband transitions, as explained more fully in Appendix I.

To proceed further we consider periodic boundary conditions. For large $N$ the eigenstates of Eqs. (2.6) and (2.7) are now given as

$$|\theta,Q\rangle_0=\left[\frac{2}{N}\right]^{1/2}\sum_{\nu\ \text{odd}}e^{i\theta(\nu+1)/2}|\nu,Q\rangle_0\ ,$$

for odd $\nu$, and

$$|\theta,Q\rangle_{1,2}=\left[\frac{2}{N}\right]^{1/2}\sum_{\nu\ \text{even}}e^{i\theta\nu/2}|\nu,Q\rangle_{1,2}\ ,$$

for even $\nu$, with $\hat{H}\,|\theta,Q\rangle=E_{\theta Q}\,|\theta,Q\rangle$,

$$E_{\theta Q}=2J[1+2\epsilon\cos Q\cos(Q-\theta)]\ . \tag{2.9}$$

In the limit $N\to\infty$ the eigenvalues form a continuum. The exact form of the spectrum has been calculated by Johnson *et al.*[13] The spectrum to first order in $\epsilon$ is depicted in Fig. 3. We note that $\theta$ plays the role of a pseudo-wave-vector which modulates the length $\nu$ of the domains in each state.

In analogy to Eq. (2.5), one can define a velocity for the propagation of a domain-wall pair in the state $|\theta Q\rangle$ as

$$V_{\theta Q}=\frac{\partial}{\partial Q}E_{\theta Q}=-4\epsilon J\sin(2Q-\theta)\ . \tag{2.10}$$

The $T=0$ spin-wave response due to transitions from the ground state to the continuum of DWP states has been calculated by IS.[9] The resulting continuum of scattering near $\omega\approx2J$ has been observed in experiments on $CsCoCl_3$ (Refs. 5 and 14–16) and $CsCoBr_3$.[11] We refer to this spectrum as the spin-wave response. The spin-wave excitation thus produced is related to the Néel state by a single spin flip if we ignore the weak admixture of the three–spin-flip state. The state reached in a spin-wave excitation therefore consists largely of a domain-wall pair of unit length. These solitons of unit length represent only a fraction of order $1/N$ of the solitons of all lengths that occur in the $2J$ manifold. The difference between the spin-wave response and the soliton response arising from the intraband transitions is illustrated in Fig. 4.

When the DWP states are thermally excited there will be a low-frequency contribution to the magnetic response from transitions within the band of excited states. Longitudinal response arises from transitions with $\Delta S^z_T=0$, and transverse response has $\Delta S^z_T=\pm1$. The intensity of such transitions taking the system from one DWP state to another will be called the soliton response. It involves initial soliton states of all lengths. From Eqs. (2.2) and (2.8) the soliton response can be written as

$$S^{zz}(Q,\omega)=\frac{4}{Z(\beta)}\sum_{\substack{\theta_1,\theta_2,\\ Q_1,Q_2}}e^{-\beta E_1}\,|\langle\theta_2,Q_2\,|\,S^z_Q\,|\,\theta_1,Q_1\rangle\,|^2\delta(\omega-E_2+E_1)\ , \tag{2.11}$$

$$S^{xx}(Q,\omega)=\frac{2}{Z(\beta)}\sum_{\substack{\theta_1,\theta_2,\\ Q_1,Q_2}}e^{-\beta E_1}(\,|\,{}_0\langle\theta_2,Q_2\,|\,S^+_Q\,|\,\theta_1,Q_1\rangle_1\,|^2+|\,{}_0\langle\theta_2,Q_2\,|\,S^+_Q\,|\,\theta_1,Q_1\rangle_2\,|^2)\delta(\omega-E_2+E_1)\ . \tag{2.12}$$

The matrix elements between the basis states are

$$ {}_0\langle \nu_2,Q_2 \mid S_Q^z \mid \nu_1,Q_1 \rangle_0 = {}_{1,2}\langle \nu_2,Q_2 \mid S_Q^z \mid \nu_1,Q_1 \rangle_{1,2} = \delta_{\nu_2,\nu_1} \left[ \left[ \frac{N}{4} \right]^{1/2} \delta_{Q_2,Q_1}\delta_{Q,\pi} - \left[ \frac{1}{N} \right]^{1/2} \delta_{Q_2,Q_1+Q-\pi} \right. $$

$$ \left. \times \exp\{i[(\nu_1-1)/2][(Q-\pi)/2]\} \frac{\sin\{\nu_1[(Q-\pi)/2]\}}{\sin[(Q-\pi)/2]} \right] , \tag{2.13} $$

and for $\nu_2$ odd, $\nu_1$ even,

$$ {}_0\langle \nu_2,Q_2 \mid S_Q^+ \mid \nu_1,Q_1 \rangle_1 = \delta_{Q_2,Q_1+Q} \left[ \frac{1}{N} \right]^{1/2} (e^{-i(Q_1+Q)}\delta_{\nu_2,\nu_1-1} + e^{iQ_1}\delta_{\nu_2,\nu_1+1}) , $$

$$ {}_0\langle \nu_2,Q_2 \mid S_Q^+ \mid \nu_1,Q_1 \rangle_2 = \delta_{Q_2,Q_1+Q} \left[ \frac{1}{N} \right]^{1/2} (e^{iQ(\nu_1-1)}\delta_{\nu_2,\nu_1-1} + e^{iQ\nu_1}\delta_{\nu_2,\nu_1+1}) . $$

Ignoring the special points $Q=\pi$ and $Q=0$,

$$ |\langle \theta_2,Q_2 \mid S_Q^z \mid \theta_1,Q_1 \rangle|^2 = \frac{1}{4N\cos^2(Q/2)} (\delta_{\theta_2,\theta_1+2Q} + \delta_{\theta_2,\theta_1})\delta_{Q_2,Q_1+Q-\pi} , \tag{2.14} $$

and

$$ |{}_0\langle \theta_2Q_2 \mid S_Q^+ \mid \theta_1Q_1 \rangle_1|^2 = \frac{2}{N}[1+\cos(2Q_1+Q-\theta_1)]\delta_{\theta_2,\theta_1}\delta_{Q_2,Q_1+Q} , $$

$$ |{}_0\langle \theta_2Q_2 \mid S_Q^+ \mid \theta_1Q_1 \rangle_2|^2 = \frac{2}{N}[1+\cos(Q+\theta_1)]\delta_{\theta_2,\theta_1+2Q}\delta_{Q_2,Q_1+Q} . \tag{2.15} $$

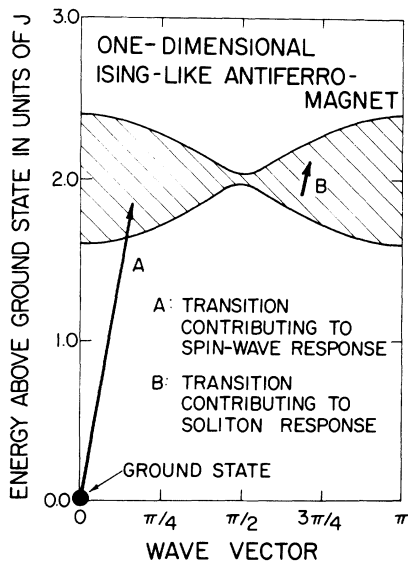


FIG. 4. Transitions contributing to the spin-wave and soliton response. Spin-wave response arises from transitions from the ground state to the band of first excited states. Soliton response arises from transitions within the band of excited states. The energy gap implies the response will be thermally activated.

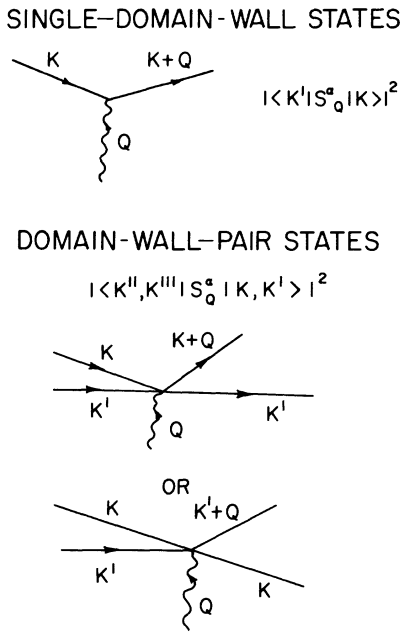


FIG. 5. Selection rules for states with a single domain wall and domain-wall–pair states. The straight lines represent propagating domain-wall states and the wavy lines represent $S_Q^\alpha$.

The squared matrix elements show that to first order in $\epsilon$, transitions contributing to the dynamic response have selection rules for two types of "momentum" transfer. The momentum $Q_1$ of a domain of given length $\nu$ propagating along the chain is changed by $Q$ ($Q-\pi$ for longitudinal response). Also, the pseudomomentum $\theta$ describing a domain changing in length either remains unchanged or changes by $2Q$. The selection rule for $\theta$ leads to a square-root singularity in the response.

It is instructive to compare the results above with those expected for states with a single domain wall such as those considered by Villain.[4] A single domain wall of momentum $K$ is coupled by $S_Q^\alpha$ to a state with momentum $K'=K+Q$. Allowing for a proper normalization of the states, the domain-wall–pair eigenstate $|\theta,Q\rangle$ can be written as a direct product of two single–domain-wall states $|K\rangle|K'\rangle\equiv|K,K'\rangle$ where $Q=K+K'$ and $\theta=2K'$. The selection rules for $\theta$ and $Q$ show that $|K,K'\rangle$ is coupled by $S_Q^\alpha$ only to the states $|K+Q,K'\rangle$ and $|K,K'+Q\rangle$ as illustrated schematically in Fig. 5. This shows that the calculation based only on domain-wall–pair states completely ignores all effects of collisions between domain walls, and is therefore equivalent to the Villain calculation. It is expected that any calculation in which the number of domain walls is conserved should yield the same result. Using (2.14) and (2.15) the soliton response can be written as

$$S^{zz}(Q,\omega)=\frac{e^{-2\beta J}}{Z(\beta)N\cos^2(Q/2)}\sum_{Q_1,\theta_1}e^{-\beta\omega_1}[\delta(\omega-\omega_A)+\delta(\omega-\omega_B)]\,,$$

$$S^{xx}(Q,\omega)=\frac{2e^{-\beta J}}{Z(\beta)N}\sum_{Q_1,\theta_1}e^{-\beta\omega_1}\{[1+\cos(2Q_1+Q-\theta_1)]\delta(\omega-\omega_B)+[1+\cos(Q_1+\theta_1)]\delta(\omega-\omega_A)\}\,, \tag{2.16}$$

where

$$\omega_1=4\epsilon J\cos Q_1\cos(Q_1-\theta_1)\,,$$

$$\omega_A=4\epsilon J\cos(Q_1-Q-\theta_1)\cos(Q_1+Q)-\omega_1\,,$$

$$\omega_B=4\epsilon J\cos(Q_1+Q-\theta_1)\cos(Q_1+Q)-\omega_1\,.$$

As $N\to\infty$ the sums are replaced by integrals,

$$\sum_{\theta_I}\to\frac{N}{4\pi}\int_{-\pi}^{\pi}d\theta_1,\quad\sum_{Q_1}\to\frac{N}{2\pi}\int_{-\pi}^{\pi}dQ_1\,,$$

leading to

$$S^{zz}(Q,\omega)=\frac{C'e^{-2\beta J}}{Z(\beta)\cos^2(Q/2)}I_1(Q,\omega)\,,$$

$$S^{xx}(Q,\omega)=\frac{2C'e^{-2\beta J}}{Z(\beta)}[I_1(Q,\omega)+I_2(Q,\omega)]\,, \tag{2.17}$$

where $C'$ is a constant and

$$I_1(Q,\omega)=\int_{-\pi}^{\pi}\int_{-\pi}^{\pi}e^{-\beta\omega_1}[\delta(\omega-\omega_A)+\delta(\omega-\omega_B)]d\theta_1dQ_1\,,$$

$$I_2(Q,\omega)=\int_{-\pi}^{\pi}\int_{-\pi}^{\pi}e^{-\beta\omega_1}[\cos(2Q_1+Q-\theta_1)\delta(\omega-\omega_B)+\cos(Q_1+\theta_1)\delta(\omega-\omega_A)]d\theta_1dQ_1\,. \tag{2.18}$$

The integrals are evaluated as

$$I_1(Q,\omega)=\begin{cases}\dfrac{8\pi I_0(2\beta\epsilon J)e^{\beta\omega/2}\cosh\left[\dfrac{\beta}{2}\cot Q(\omega_Q^2-\omega^2)^{1/2}\right]}{(\omega_Q^2-\omega^2)^{1/2}} & \text{for } |\omega|<\omega_Q\,,\\ 0 \text{ for } |\omega|>\omega_Q\end{cases}$$

$$I_2(Q,\omega)=\begin{cases}-8\pi I_0(2\beta\epsilon J)e^{\beta\omega/2}\dfrac{\sinh\left[\dfrac{\beta}{2}\cot Q(\omega_Q^2-\omega^2)^{1/2}\right]}{|\omega_Q|} & \text{for } |\omega|<\omega_Q\,,\\ 0 \text{ for } |\omega|>\omega_Q\end{cases} \tag{2.19}$$

where $I_0(x)$ is the modified Bessel function and $\omega_Q = 4\epsilon J \sin Q$. Using Eqs. (2.17) and (2.19) we find the contribution to the soliton scattering from transitions within the first band of excited states is

$$S^{zz}(Q,\omega) = \frac{Ce^{-2\beta J} I_0(2\beta\epsilon J) e^{\beta\omega/2} \cosh\left[\frac{\beta}{2}\cot Q(\omega_Q^2-\omega^2)^{1/2}\right]}{Z(\beta)\cos^2(Q/2)(\omega_Q^2-\omega^2)^{1/2}}$$

and

$$S^{xx}(Q,\omega) = \frac{2Ce^{-2\beta J} I_0(2\beta\epsilon J) e^{\beta\omega/2}}{Z(\beta)} \left[ \frac{\cosh\left[\frac{\beta}{2}\cot Q(\omega_Q^2-\omega^2)^{1/2}\right]}{(\omega_Q^2-\omega^2)^{1/2}} - \frac{\sinh\left[\frac{\beta}{2}\left|\frac{\cos Q}{\sin Q}\right|(\omega_Q^2-\omega^2)^{1/2}\right]}{|\omega_Q|} \right] \quad \text{for } |\omega| < \omega_Q \,. \tag{2.20}$$

$S^{zz} = S^{xx} = 0$ for $|\omega| > \omega_Q$, where $C$ is a constant. The result for $S^{zz}(Q,\omega)$ has the same spectral response as that obtained by Villain.[4] The result for $S^{xx}(Q,\omega)$ is new.

Since the calculation above neglects the effects of collisions it is expected that the spectral response will be the same as that arising from states with only one domain wall. With the present derivation, however, the soliton response and the spin-wave response can be understood in a unified way. The spin-wave response arises from transitions from the ground state to those members of the band of first excited states which consist primarily of linear combinations of domain-wall–pair states of unit length. The soliton scattering arises from transitions within the thermally populated band of excited domain-wall–pair states of any length; in the process the soliton changed its length by $\pm 1$ or 0.

Equation (2.20) for the soliton response shows that both $S^{zz}(Q,\omega)$ and $S^{xx}(Q,\omega)$ have square-root singularities at the cutoff frequency $\omega_Q$. Figure 6 shows the calculated line shape of a neutron scattering experiment at $Q = \pi/2$ where $S^{zz}(Q,\omega) = S^{xx}(Q,\omega)$. The observed scattering is proportional to the convolution of $S^{\alpha\alpha}(Q,\omega)$ with the spectrometer resolution function,

$$I(Q,\omega) \propto \int S(Q,\omega') R(\omega-\omega') d\omega' \,. \tag{2.21}$$

Here a Gaussian was used to simulate frequency resolution. Note the well-defined peak expected at $\omega = \omega_Q$, the Villain mode frequency.

The soliton scattering Eq. (2.20) has other characteristic behavior. The scattering is thermally activated. Note that, although the expression (2.20) gives the soliton scattering within the manifold at $\omega \approx 2J$ and has a temperature factor of the form $e^{-2\beta J}/Z(\beta)$, the observed scattering intensity is the sum of scattering due to transitions within all of the excited-state manifolds. For open chains or rings at low temperatures the leading-order temperature dependence is then expected to be proportional to $e^{-\beta J}$ independent of the boundary condition. Our experiments are consistent with this result.

Another feature of the response is that the integrated intensity of the longitudinal component diverges as $Q \to \pi$, while the intensity of the transverse component is only weakly dependent on $Q$. These predictions can be checked experimentally.

As discussed by Villain, the square-root singularities are expected to be rounded by collisions. This corresponds to including higher-order terms in the perturbation theory presented above. The collective mode at $\omega_Q$ has strong scattering because of the selection rules for the pseudomomentum $\theta$. Were it not for the fact that the $\theta$ operator commutes with $\hat{H}$, the square-root singularities would be broadened. Indeed, one expects that if higher-order terms are included, the energy eigenstates will no longer be characterized by $\theta$. An illustrative example where the eigenstates are no longer states of constant $\theta$ is when $\hat{H}$ includes a uniform staggered field. The eigenstates then form the "Zeeman ladder" discussed by Shiba[17] and the low-frequency scattering appearing at elevated temperatures corresponds to transitions between states in the ladder. Figure 7 shows a calculation of $S^{zz}(Q,\omega)$ done by numerically diagonalizing the Hamiltonian equation (2.8) for an array of 40 spins. The resulting histograms have been convoluted with a Gaussian resolution of full width at half maximum (FWHM) of 0.18 THz to produce the line shapes shown. Qualitatively it is apparent that the

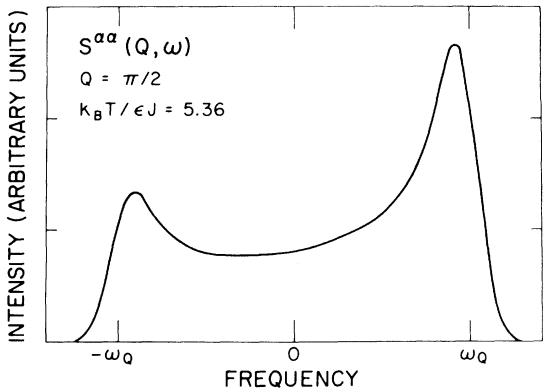


FIG. 6. Line shape due to soliton scattering at the zone boundary $Q = \pi/2$; $\omega_Q = 4\epsilon J \sin Q$ is the Villain mode frequency as described in the text.

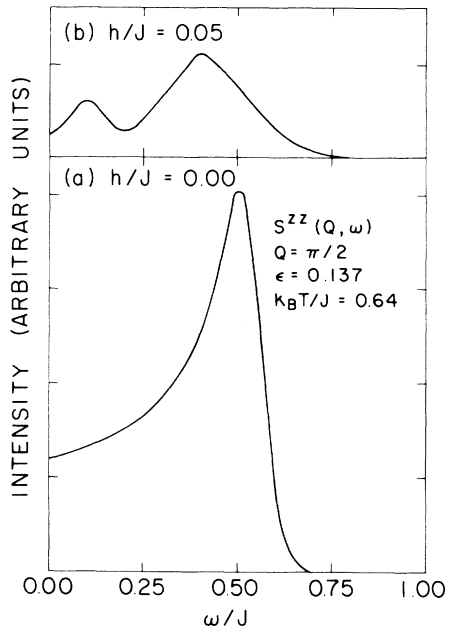


FIG. 7. Numerical calculation of $S^{zz}(Q,\omega)$ as described in the text. (a) No staggered field. (b) In the presence of the uniform staggered field $h/J=0.05$.

extra term $h\sum_i(-1)^i S_i^z$ causes the main Villain mode peak to broaden considerably and shifts more spectral weight to lower frequencies. The intensity is also dramatically reduced. This may explain why the soliton scattering was not observed in an early experiment at $T\simeq T_{N_1}$ where the interchain field is large [J. Rossat-Mignod, (private communication)].

The theory discussed so far is not expected to be valid very near to a zone center.[4] At the zone center the time between collisions of moving domain walls is much shorter than $1/\omega_Q$, the characteristic scattering frequency.

### A. Long wavelengths

Maki[10] discussed the longitudinal scattering near $Q=\pi$, and suggested that, if the system is approximated by a $\phi^4$ model, the correlation functions may be calculated in the ideal–soliton-gas limit.

Using the Villain expression for the energy of a soliton Maki[10] calculated the total soliton density as

$$\bar{n}_s=\tfrac{1}{2}e^{-\beta J}I_0(2\beta\epsilon J)\ , \tag{2.22}$$

and the thermal soliton velocity as

$$v_0=\frac{4\sinh(2\beta\epsilon J)}{\pi\beta I_0(2\beta\epsilon J)}\ . \tag{2.23}$$

When $|Q-\pi|\ll\pi$ the longitudinal correlation function can be written approximately as

$$S^{zz}(Q,\omega)=\frac{4\pi\bar{n}_s}{v_0}\left[(Q-\pi)^2+4\bar{n}_s^2+\left[\frac{\omega}{v_0}\right]^2\right]^{-3/2}\ . \tag{2.24}$$

The line shape is similar to that describing the soliton scattering of a classical (1D) planar antiferromagnet in a magnetic field.[3] The characteristic temperature dependence and non-Lorentzian line shape can also be checked experimentally on the Ising-type antiferromagnet near the antiferromagnetic zone center.

## III. EXPERIMENT

The single crystal of $CsCoBr_3$ was described previously.[11] $CsCoBr_3$ has a hexagonal structure $c=6.261$ Å, $a=7.445$ Å, with chains of magnetic $Co^{2+}$ ions along the $c$ axis. There are two $Co^{2+}$ ions per unit cell, and above the 3D ordering temperature ($T_{N_1}=28.3$ K) (Ref. 18) the cobalt spins lie predominantly along the chain direction.

The $CsCoBr_3$ crystal was aligned so that its $(h,o,l)$ plane lay in the scattering plane of the N5 triple-axis spectrometer at the NRU reactor, Chalk River. A neutron beam reflected from a Si(111) monochromator and collimated to 0.6° was scattered by the specimen through a 0.7° collimator for analysis by a Si(111) analyzer operating at fixed scattered-neutron energy $E_1$. For most scans $E_1/h$ was 3 THz.

For a 1D system with an easy axis in the $c$ direction, the magnetic scattering intensity is given by

$$I(\vec{\kappa},\omega)\propto V_{\vec{\kappa}}^{\text{eff}}f(\vec{\kappa})^2[\sin^2\Phi S^{zz}(Q,\omega)+(1+\cos^2\Phi)S^{xx}(Q,\omega)]\ , \tag{3.1}$$

where $2Q/c=\vec{\kappa}\cdot\hat{z}\equiv\kappa\cos\Phi$, $f(\vec{\kappa})$ is the magnetic form factor, and $V_{\vec{\kappa}}^{\text{eff}}$ is the effective volume correcting for self-absorption of neutrons.

The strategy for observing the low-frequency magnetic scattering was as follows. Constant $\vec{\kappa}$ scans were performed at various wave vectors at a temperature of 5 K, where the scattering is dominated by the nuclear incoherent scattering (NIS) centered at $\omega=0$, plus a fast neutron background extending to higher frequencies. The intensity of the NIS at a given wave vector $\vec{\kappa}$ was taken as a measure of $V_{\vec{\kappa}}^{\text{eff}}$. The same scan was repeated at higher temperatures, and the smoothed 5-K background was subtracted from the data. The strong intensity of the NIS at $\omega=0$ restricted the measurements of the thermally activated magnetic scattering to frequencies greater than 0.15 THz. Figure 8 shows some typical raw data scans. The lines have been drawn as guides to the eye. The intensity increases markedly at elevated temperatures because of the thermal excitation of domain-wall pairs. An inelastic peak is observed at 50 K. By 80 K the region below the peak has filled in as the domain-wall density is now high enough for collisions to take place. A summary of some of the scans performed and the effective volumes measured is contained in Table I.

## IV. RESULTS AND DISCUSSION

Some 50-K data from which the 5-K smoothed background has been subtracted are shown in Figs. 9–11. The scattering profiles show a definite peak whose frequency decreases from its zone-boundary value of 0.89±0.07 THz. If the peak is present in the (1.2,0,0.93) scan, the

TABLE I. Information used to analyze the soliton scattering into transverse and longitudinal components according to Eq. (3.1). The symbols are defined in the text.

| Wave-vector transfer $\vec{\kappa}$ | Effective volume $V_{\vec{\kappa}}^{\text{eff}}$ | (Form factor)$^2$ $f(\vec{\kappa})^2$ | Transverse strength $1+\cos^2\Phi$ | Longitudinal strength $\sin^2\Phi$ | Temperatures of measurements $T$ (K) |
|---|---|---|---|---|---|
| (0,0,1.07) | 0.94 | 0.88 | 2.00 | 0.00 | 5,80 |
| (0,0,1.2) | 1.06 | 0.85 | 2.00 | 0.00 | 5,50,80 |
| (0,0,1.3) | 1.16 | 0.83 | 2.00 | 0.00 | 5,80 |
| (0,0,1.4) | 1.05 | 0.81 | 2.00 | 0.00 | 5,80 |
| (0.3,0,1.5) | 1.00 | 0.78 | 1.96 | 0.04 | 5,50,80 |
| (1.2,0,0.5) | 1.56 | 0.84 | 1.16 | 0.84 | 5,35,50,80 |
| (1.2,0,0.6) | 1.40 | 0.83 | 1.21 | 0.79 | 5,50,80 |
| (1.2,0,0.7) | 1.36 | 0.82 | 1.27 | 0.73 | 5,35,50,80 |
| (1.2,0,0.8) | 1.37 | 0.80 | 1.32 | 0.68 | 5,50,80 |
| (1.2,0,0.93) | 1.30 | 0.78 | 1.42 | 0.588 | 5,35,50,80 |
| (2.2,0,0.6) | 1.19 | 0.56 | 1.07 | 0.93 | 5,80 |
| (2.2,0,0.8) | 1.25 | 0.56 | 1.12 | 0.88 | 5,80 |

frequency is too low to be detected in this experiment. From Fig. 9 we see that the peak at (0.3,0,1.5) occurs at the same frequency as the (1.2,0,0.5) zone boundary. The (0.3,0,1.5) scan is 98% transverse response, while the (1.2,0,0.5) scan is 42% longitudinal response. The fact that the peak occurs at the same place is in agreement with the prediction of Eq. (2.20). The dispersion of the observed peak is plotted in Fig. 12. The solid line is the Villain mode frequency, $\omega_Q = 4\epsilon J \sin Q$, with $J=1.62$ THz and $\epsilon=0.137$. The parameters were independently determined from spin-wave measurements and an extended version of the IS theory that takes account of exchange mixing and 3D correlations.[11] The observed peak frequencies are consistent with the expected $\sin Q$ dispersion law.

The scattering is thermally activated as shown in Fig. 13. Table II shows the integrated intensities above background at (1.2,0,0.5) for 35, 50, and 80 K as well as the ratios normalized to 50 K. It is apparent that the data are reasonably described by a temperature factor $e^{-\beta J}$ with $J=1.62$ THz. As discussed above this is the expected temperature dependence arising from summing over all manifolds of energy $nJ$ independent of whether open

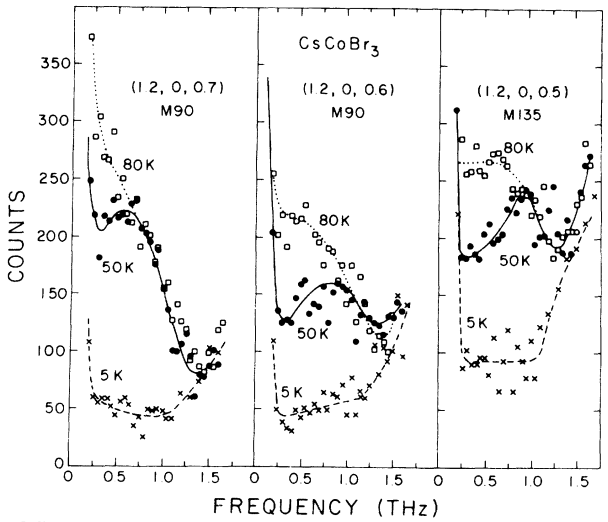


FIG. 8. Thermally activated scattering in $CsCoBr_3$. The monitor value following letter $M$ is a measure of the number of incident neutrons.

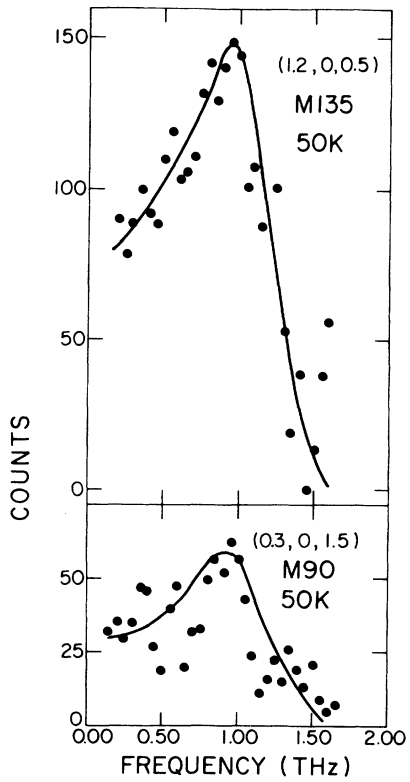


FIG. 9. Scattering above background at the antiferromagnetic zone boundary at 50 K. The lines are guides to the eye.

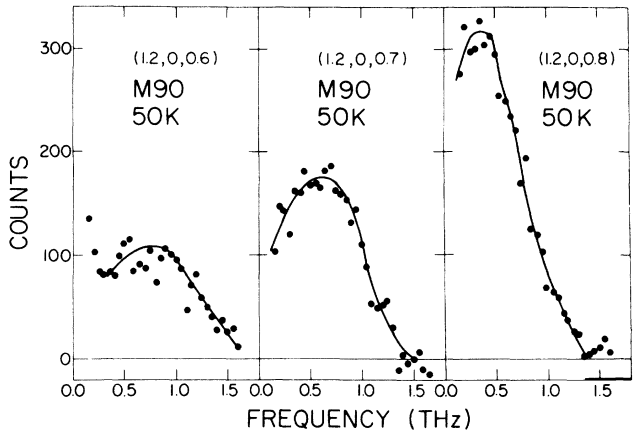


FIG. 10. Scattering above background at 50 K. Note how the peak frequencies decrease as $\eta \rightarrow 1$, i.e., as $Q \rightarrow \pi$.

(chain) or periodic (ring) boundary conditions are used.

When allowance is made for $V_{\vec{\kappa}}^{\text{eff}}$, $f(\vec{\kappa})^2$, and the polarization factor, measurements at two values of $\vec{\kappa}$ with equivalent values of $Q=\vec{\kappa}\cdot\hat{z}c/2$ can be combined so as to extract the longitudinal and transverse parts of $S(Q,\omega)$. The smoothed line-shape profiles obtained in this way at $Q=\pi/2$ are shown in Fig. 14. The wave vectors used were (1.2,0,0.5) and (0.3,0,1.5). According to Eq. (2.20) the transverse and longitudinal responses at the zone boundary are identical. The experimental results of Fig. 14 are certainly consistent with this prediction in overall shape and intensity.

The experimental integrated intensities of the soliton scattering at all wave vectors were determined by measuring the areas under the smoothed line-shape profiles and applying the condition for detailed balance, $S(Q,-\omega)=e^{-\beta\omega}S(Q,\omega)$, to obtain the scattering at neutron energy gain. The intensity near $\omega=0$ was estimated by interpolation. From the pairs of intensities, the observed weights of the transverse and longitudinal scattering were extracted at five values of $Q$ ranging from $0.5\pi$ to $0.93\pi$. The results at 80 K are plotted in Fig. 15, normalized to the results at $Q=\pi/2$. The solid lines represent the same quantities calculated by integrating Eq. (2.20) from $-\omega_Q$ to $\omega_Q$, using $J$ and $\epsilon$ as above. The theoretical results are quite consistent with the experiment. The transverse intensity is only slightly $Q$ dependent, while the longitudinal intensity shows a marked rise as $Q$ tends towards the antiferromagnetic zone center. The observed longitudinal intensity at $Q=0.93\pi$ is large but still well below the theoretical prediction. As noted by Villain,[4] the $1/\cos^2(Q/2)$ dependence in Eq. (2.20) is likely a spurious result of the first-order theory. Villain argued that the true dependence should have the form $(\frac{1}{4})\kappa_c^2+\cos^2(Q/2)$ to obtain agreement with the known $S^{zz}(Q)$ of the 1D Ising model. This removes the divergence of the longitudinal intensity for $|Q-\pi| \ll \kappa_c$, the inverse correlation length, for $\kappa_c \neq 0$.

Figure 16 shows the intensity ratio of the longitudinal to transverse soliton intensities as a function of $Q$. There are no adjustable parameters in the calculation shown by the solid line. As expected, the calculated ratio near $Q=\pi$ is too large but otherwise the results are in reasonable agreement with the experiment.

With the same experimental setup, the spin-wave scattering of $CsCoBr_3$ was also measured at the zone boundary (0,0,2.5) in order to find the ratio of the soliton to the spin-wave scattering. One can then obtain the quantity

$$R_Q = S^{zz}(Q)/S^{xx}(Q)$$

where

$$S^{zz}(Q) = \int_{-\infty}^{\infty} d\omega\, S^{zz}(Q,\omega) .$$

At 50 K, the experimentally deduced value including the soliton and spin-wave scattering is $R_{\pi/2}=0.6$. This can be compared with the value expected for a pure Ising model, which is given by

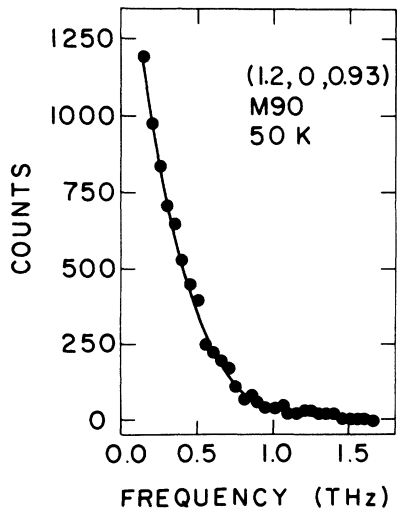


FIG. 11. Scattering above background near $Q=\pi$ at 50 K.

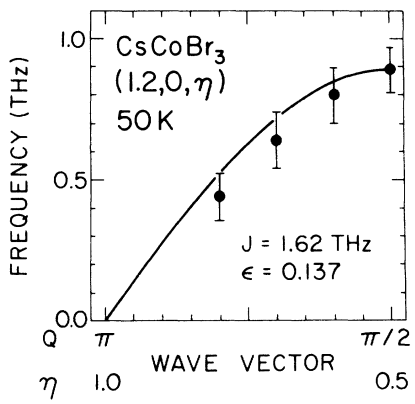


FIG. 12. Dispersion of the Villain mode. The solid line is $\omega_Q=4\epsilon J \sin Q$ using the known $\epsilon$ and $J$ which describe the spin-wave response in $CsCoBr_3$.

TABLE II. Integrated intensity ratios at (1.2,0,0.5).

| $T$ (K) | Integrated intensity $I_T$ (arbitrary units) | $\frac{I_T}{I_{50}}$ | $\frac{e^{-\beta j}}{e^{-\beta J}\mid_{50}}$ | $\frac{e^{-2\beta J}}{e^{-2\beta J}\mid_{50}}$ |
|---|---|---|---|---|
| 35 | 2282 | 0.48 | 0.51 | 0.26 |
| 50 | 4768 | 1.00 | 1.00 | 1.00 |
| 80 | 7257 | 1.52 | 1.79 | 3.21 |

$$R_Q^I=\frac{1-\exp(-2\kappa_c)}{1+2\exp(-\kappa_c)\cos Q+\exp(-2\kappa_c)} ,$$

where $\kappa_c=-\ln[\tanh(J\beta/2)]$. With the known $J$ of 1.62 THz, we calculate $R^I_{\pi/2}=0.40$ at 50 K. Thus the observed intensity of the soliton scattering bears approximately the correct relation to the intensity of the spin-wave scattering. The small disrepancy that remains suggests that the theory underestimates the soliton contribution.

In Fig. 13 which showed the 50-K scattering observed at (1.2,0,0.5) and (1.2,0,0.7), the theoretical lines represent the convolution of $I(\vec{\kappa},\omega)$ [Eq. (2.20)] with a Gaussian resolution function of FWHM 0.18 THz. The observed scattering is much broader than predicted by theory. Some broadening of the square-root singularity is expected from collisions between domain walls. The collisional effects should increase with temperature. Figures 17 and 18 show scattering profiles at three temperatures for the wave vectors (1.2,0,0.5) and (1.2,0,0.7). The results at both wave vectors share common features. At 35 K the peak in the scattering is sharp and well defined. When the temperature is raised to 50 K the peak is visible but clearly broadened.

Between 50 and 80 K a qualitative change takes place: Much of the intensity occurs at lower frequencies and the peak is rounded off into a sloping shoulder. The dashed lines in Fig. 17 represent the imaginary part of the susceptibility as determined from the smoothed scattering line shapes with the relation $\chi''(Q,\omega)=(1-e^{-\beta\omega})S(Q,\omega)$. The peak in the susceptibility also broadens and changes shape with increasing temperature, showing that the temperature dependence does not arise simply from variations of the thermal population factor. Results at $Q=0.6\pi$ and $0.8\pi$ have the same behavior. The exact calculations of IS (Ref. 9) of $S^{\alpha\alpha}(Q,\omega)$ for rings of 10 spins are in qualitative agreement with this behavior. The exact calculations contain the collisional effects and are indicative of the behavior of the infinite chain.

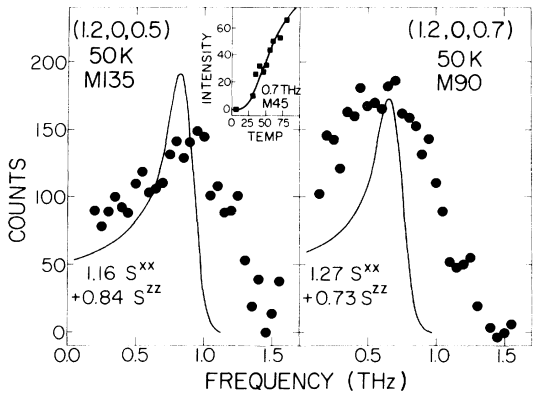


FIG. 13. Comparison of the observed scattering above background at $Q=\pi/2$ and $Q=7\pi/10$ with the theoretical curves described in the text. Inset: temperature scan at (1.2,0,0.5).

At present, however, there is no analytic theory that explains the temperature dependence of the scattering. Such a theory would presumably have to include the coupling by the Hamiltonian equation (2.3) of states with $p$ domain walls to states with $p\pm2$ walls.

At the wave vector $Q=0.93\pi$ the ideal–soliton-gas theory of Maki[10] should be applicable. The transverse and longitudinal soliton scattering are expected to have the same shape (but not the same intensity). As the scattering at (1.2,0,0.93) is dominated by $S^{zz}(Q,\omega)$, we compare the observed scattering to Maki's theory, Eq. (2.24):

$$[S^{zz}(Q,\omega)]^{-2/3}=A\omega^2+B , \tag{4.1}$$

where

$$A=(4\pi\bar{n}_s v_0^2)^{-2/3}$$

and

$$B=\left[\frac{4\pi\bar{n}_s}{v_0}\right]^{-2/3}[(Q-\pi)^2+4\bar{n}_s^2] .$$

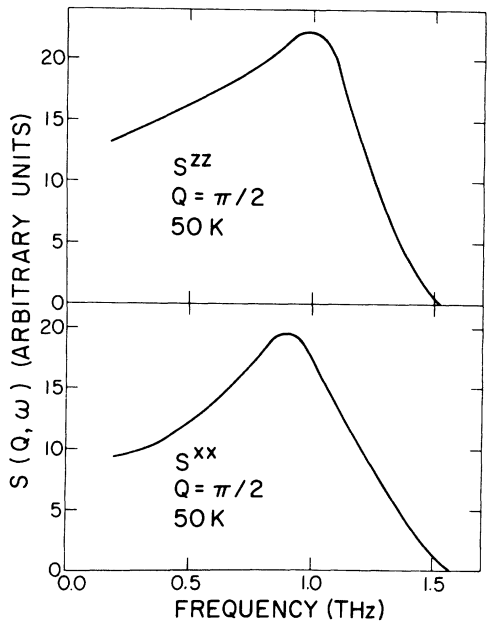


FIG. 14. Smoothed experimental profiles of $S^{zz}(Q,\omega)$ and $S^{xx}(Q,\omega)$ observed at $Q=\pi/2$ and a temperature of 50 K.

Figure 19 shows a plot of (intensity)$^{-2/3}$ against squared frequency $\nu^2(\nu=\omega/2\pi)$ for 35, 50, and 80 K. The lines are the result of a weighted least-squares fit. For frequencies less than 0.5 THz the data can be described well by Eq. (4.1). However, a Lorentzian distribution yields a fit that is almost as good. The present experiment does not lead to a definitive distinction between the two functions. It is probably necessary to obtain measurements over a wider range of values of frequency, but such measurements will be difficult and time consuming. Maki's theory, however, is very suggestive, and the temperature dependence is qualitatively correct.

Equation (2.24) can also be written in the form

$$S^{zz}(Q,\omega)=\frac{c}{(\Gamma^2+\omega^2)^{3/2}} ,$$

where

$$\Gamma=v_0(4\bar{n}_s^2+(Q-\pi)^2)^{1/2} ,$$
$$c=4\pi\bar{n}_s v_0^2 . \tag{4.2}$$

These quantities are related to Eq. (4.1) by

$$\Gamma=(B/A)^{1/2},\quad c=A^{-3/2} .$$

From Eqs. (2.22) and (2.23) with the known $\epsilon=0.137$ and $J=1.62$ THz, $\Gamma$ and $c$ can be calculated with no adjustable parameters. Table III gives a summary of the calculated and fitted values for $Q=0.93\pi$, normalized to the values at 50 K. The theoretical and fitted experimental ratios are in excellent agreement. The width $\Gamma$ and "energy density" $c$ both increase with temperature as predicted by Eq. (2.24). The ratios provide evidence that the ideal–soliton-gas picture is valid for the $S=\frac{1}{2}$ Ising-type antiferromagnetic chain near $Q=\pi$. However, the calculated absolute value of $\Gamma$ is a factor of about 2.4 $[\approx(2\pi)^{1/2}]$ smaller than the observed value. More work is also necessary to determine whether or not the line shape is truly non-Lorentzian. It is also desirable to check the variation of $\Gamma$ with $Q$. At 35 K the theoretical value of $\Gamma$ at $Q=\pi$ is about half as large as $\Gamma$ at $Q=0.93\ \pi$. It should be possible to check this experimentally. At the

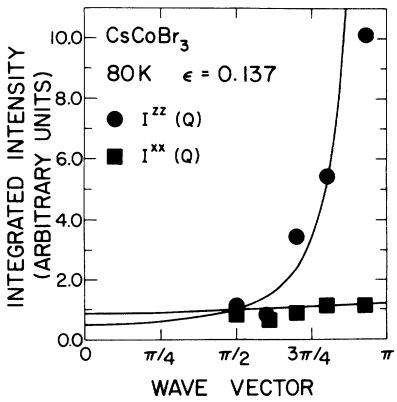


FIG. 15. Integrated intensity of the soliton scattering at 80 K as a function of $Q$. The theoretical and observed intensities have been normalized to the value of $I^{zz}$ at the zone boundary $Q=\pi/2$.

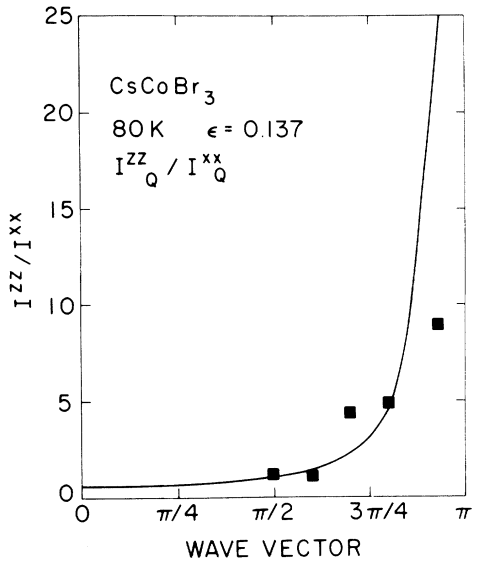


FIG. 16. Integrated intensity ratios of longitudinal to transverse scattering at 80 K. The theoretical line is described in the text.

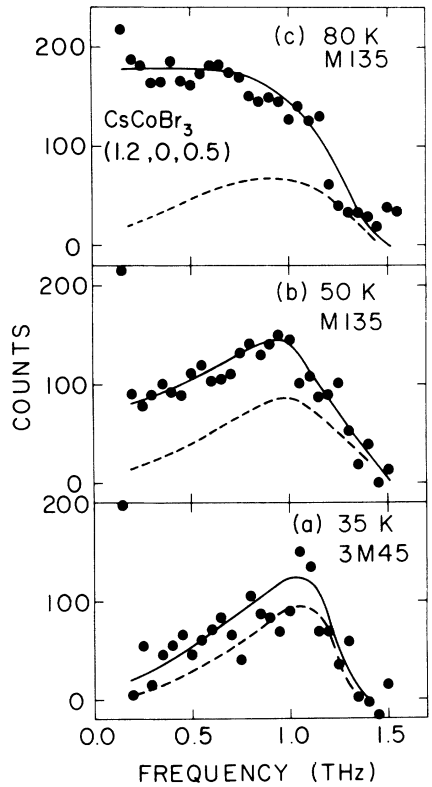


FIG. 17. Increasing effect of collisions with temperature at the zone boundary (1.2,0,0.5). Scattering above background at (a) 35 K, (b) 50 K, and (c) 80 K. The 35-K data measured at monitor 45 has been multiplied by 3 for comparison with the other data. The solid lines are guides to the eyes. The dashed lines represent $\chi''(Q,\omega)$ as described in the text.

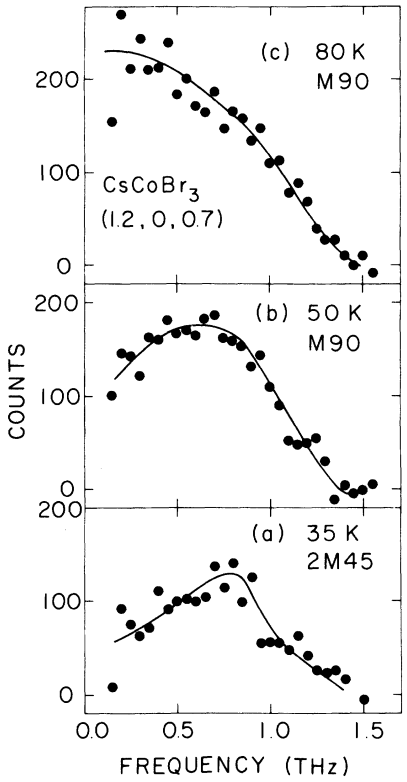


FIG. 18. Increasing effect of collisions with temperature at (1.2,0,0.7). Scattering above background at (a) 35 K, (b) 50 K, and (c) 80 K. The solid lines are guides to the eye.

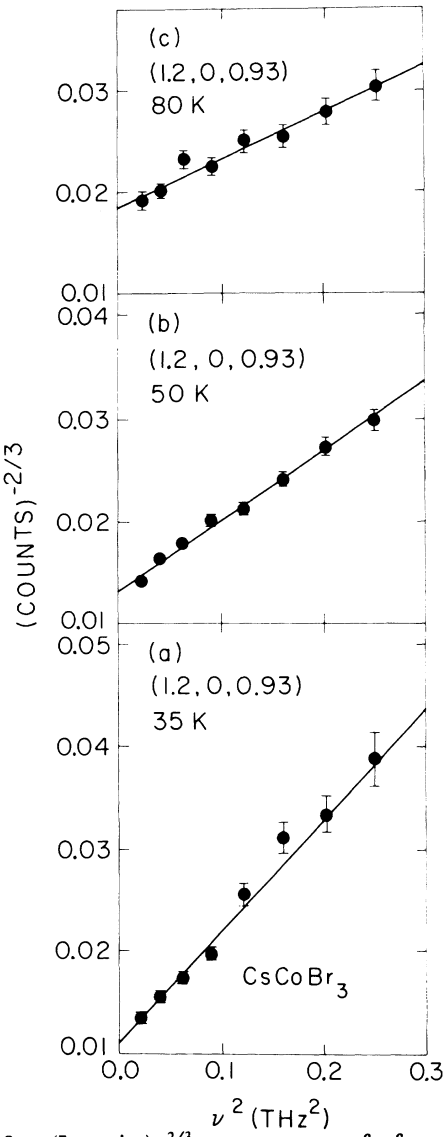


FIG. 19. (Intensity)$^{-2/3}$ vs square of frequency at $Q=(1.2,0,0.93)$. (a) 35 K, (b) 50 K, and (c) 80 K. The solid lines are results of least-squares fits to the data as described in the text.

present it can only be concluded that, with the limited data available, the $\frac{3}{2}$ power law for the spectrum is consistent with experiment.

## V. CONCLUDING REMARKS

The dynamic soliton response of the 1D $S=\frac{1}{2}$ Ising-type antiferromagnet has been calculated to first order in $\epsilon$. The result for the longitudinal scattering agrees with the calculation of Villain. The result for the transverse soliton response is new.

Experiments on $CsCoBr_3$ have revealed that at elevated temperatures a low-frequency component of the magnetic response appears with a well-defined inelastic peak. The peak shows that there exists a propagating collective mode in the soliton gas. The dispersion of the peak, as well as the intensity and polarization of the scattering, can be reasonably described by the theory, using parameters determined independently from spin-wave measurements. The scattering is broader than predicted by the theory. This may be expected on the basis of collisions, and the measurements confirm the increasing effect of collisions with temperature. The detailed behavior is, however, still not well understood theoretically.

Finally, the response near $Q=\pi$ has been compared with Maki's theory based on a gas of solitons. The experimental results at different temperatures are consistent with the spectral form and intensity predicted by the theory.

*Note added*: Recent calculations have been made of the soliton response at $Q=\pi$ for a ring of 12 spins by T. Schneider and E. Stoll [Phys. Rev. B 26, 3846 (1982)]. Their histogram spectrum extends to about 0.4 THz so that detailed comparison, in the region where most of the data exists, cannot be made at present.

## ACKNOWLEDGMENTS

The expert technical assistance of J. C. Evans, M. M. Potter, D. C. Tennant, and H. F. Nieman is gratefully acknowledged. We thank G. E. Lee-Whiting and T. Schneider for useful discussions. One of the authors (S.E.N.) was supported by a Natural Sciences and Engineering Research Council (Canada) postgraduate scholarship.

TABLE III. Fitted and calculated parameters in the Maki theory.

| Temperature | 35 K | 50 K | 80 K |
|---|---|---|---|
| $\Gamma$ (calculated) | 0.14 THz | 0.17 THz | 0.25 THz |
| $\Gamma$ (fitted) | 0.32 THz | 0.43 THz | 0.62 THz |
| $\Gamma/\Gamma_{50}$ (fitted) | 0.74 | 1.00 | 1.44 |
| $\Gamma/\Gamma_{50}$ (calculated) | 0.79 | 1.00 | 1.43 |
| $c/c_{50}$ (fitted) | 0.52 | 1.00 | 1.79 |
| $c/c_{50}$ (calculated) | 0.52 | 1.00 | 1.77 |

## APPENDIX I: BOUNDARY CONDITIONS IN THE TIGHT-BINDING MODEL

In first-order perturbation theory the Hamiltonian for the Ising-type chain, Eq. (2.8), is formally equivalent to a nearest-neighbor tight-binding model with one free end.[9] The local energy is equivalent to $2J$ and the nearest-neighbor transfer is given by $V_{Q_1}$. Position $r$ in the tight-binding model is related to domain size $\nu$. For odd-length domains, $\nu=1,3,\ldots,\ r=(\nu+1)/2$. In particular, the domain of length $\nu=1$, which has one spin flipped from the Néel state, corresponds to the surface term $r=1$.

The spin-wave response at $T=0$ arises from transitions from the ground state to the first excited states, coupled by matrix elements of the form $|\langle E|S_Q^+|G\rangle|^2$. Since the first-order ground state is only slightly different from the Néel state, the surface term $\nu=1$ dominates the spin-wave response. The open-ended boundary condition is therefore essential for calculating the spin-wave scattering.

On the other hand, for the soliton response arising from transitions within the band of excited states, the contribution of the surface states is only $O(1/N)$. The boundary condition is thus not important in the $N\rightarrow\infty$ limit.

The decreasing importance of the boundary condition as $N$ becomes large has been verified by calculations of the response to order $\epsilon$ for chains of length up to 80 spins, with periodic and open boundary conditions.

Because the spin-wave states comprise only $O(1/N)$ of the thermally excited states, it is clear that in the Ising-type system the thermally activated scattering is dominated by solitons. This is not the case for $XY$ and Heisenberg systems, where two-magnon scattering can make an appreciable contribution.[19]


[1]H. J. Mikeska, J. Appl. Phys. 52, 1950 (1981).
[2]J. K. Kjems and M. Steiner, Phys. Rev. Lett. 41, 1137 (1978).
[3]L. P. Regnault, J. P. Boucher, J. Rossat-Mignod, J. P. Renard, J. Bouillot, and W. G. Stirling, J. Phys. C 15, 1261 (1982).
[4]J. Villain, Physica 79B, 1 (1975).
[5]H. Yoshizawa, K. Hirakawa, S. K. Satija, and G. Shirane, Phys. Rev. B 23, 2298 (1981).
[6]S. E. Nagler, W. J. L. Buyers, R. L. Armstrong, and B. Briat, Phys. Rev. Lett. 49, 590 (1982).
[7]H. Shiba and K. Adachi, J. Phys. Soc. Jpn. 50, 3278 (1981).
[8]K. Adachi, J. Phys. Soc. Jpn. 50, 3204 (1981).
[9]N. Ishimura and H. Shiba, Prog. Theor. Phys. 63, 743 (1980).
[10]K. Maki, Phys. Rev. B 24, 335 (1981).
[11]S. E. Nagler, W. J. L. Buyers, R. L. Armstrong, and B. Briat, Phys. Rev. B 27, 1784 (1983).
[12]J. Villain, in *Ordering in Strongly Fluctuating Condensed Matter Systems*, edited by T. Riste (Plenum, New York, 1980), p. 91.
[13]J. D. Johnson, S. Krinsky, and B. M. McCoy, Phys. Rev. A 8, 2516 (1973).
[14]W. J. L. Buyers, J. Yamanaka, S. E. Nagler, and R. L. Armstrong, Solid State Commun. 33, 867 (1980).
[15]S. K. Satija, G. Shirane, H. Yoshizawa, and K. Hirakawa, Phys. Rev. Lett. 44, 1548 (1980).
[16]S. E. Nagler, R. L. Armstrong, and W. J. L. Buyers, J. Appl. Phys. 52, 1971 (1981).
[17]H. Shiba, Prog. Theor. Phys. 64, 466 (1980).
[18]W. B. Yelon, D. E. Cox, and M. Eibschütz, Phys. Rev. Lett. B 12, 5007 (1975).
[19]G. Reiter, Phys. Rev. Lett. 46, 1981 (1981).